Physics of Transition to Annular Flow in Microchannel Flow Boiling Process

Meisam Habibimatin, Abdolreza Fazeli, Saeed Moghaddam*
Department of Mechanical and Aerospace Engineering,
University of Florida
Gainesville, Florida, United States, 32611
*Email: saeedmog@ufl.edu

ABSTRACT

Transition to annular flow regime in microchannels is arguably one of the most complex phenomena in the flow boiling process. The instability of the vapor-liquid interface in this interstitial regime presents an intricate situation in which the interface pattern rapidly changes with the mass flow rate and surface heat flux. Although a few past studies have reported observing this regime, thermohydraulics of the process and flow and boundary conditions under which this transition occurs have remained largely unknown. The main obstacle in deciphering the physics of this process has been the lack of measurement tools to characterize hydrodynamics and thermal characteristics of this flow regime. The present study benefits from a novel test device that enables measuring the liquid film thickness and velocity with unprecedented spatial and temporal resolutions. Our experimental results show that each flow regime has a unique thermal signature associated with the onset of the liquid film flow. This can be considered as the most fundamental mechanistic-based transition criterion.

KEY WORDS: Flow Boiling, Microchannel, Annular Flow

NOMENCLATURE

x	Axial coordinate
T	Temperature, °C
V	Velocity, m/s
k	Thermal conductivity, W/m.K

Greek symbols

δ	Liquid thickness (μm)

Subscripts

s	Surface
L	Liquid

INTRODUCTION

Over the past decade, there has been significant research focused on understanding and enhancing the flow boiling process in microchannels [1-15]. It is commonly accepted that the thermal performance of a two-phase microchannel heat sink is governed by the prevailing flow regime. This trend has encouraged extensive investigations on different flow regimes and their respective transition criteria [16-22] and thermal characteristics. It is common knowledge that bubbles rapidly grow and occupy most of the microchannel cross-section. In this process, a thin liquid layer is trapped between the bubble and microchannel walls. At relatively low vapor velocities, strong shear forces generated due to thinness of the liquid layer prevent the liquid layer from moving along the microchannel. However, high vapor velocities subject the liquid layer to strong shear forces resulting in its motion, and hence transition to the annular flow regime. Finding a criterion for this transition has proven to be extremely difficult. The flow regime map proposed by Revellin and Thome [18] suggests that transition from the elongated bubble regime to annular regime occurs in a broad range of vapor quality and mass flux.

The similarity of the annular regime to other interstitial (transitional) regimes such as churn and slug-annular, chaotic behavior and instability of the interface at the transition region and abruptness of this transition are among the sources of difficulties in defining a transition criterion [18, 21]. The literature even lacks a consensus on identity of the transitional regimes. For example, a nearly identical flow pattern is called churn regime by Tibirica [23] and semi-annular regime by Chang et al. [24]. In another study by Triplett et al. [25], no criteria are introduced for transition from elongated bubbles to annular flow regime. This lack of consensus on identifying the transitional regime stems from the absence of an explanation for the physics of the transition process. The two major works that investigated the effect of channel size on transition from elongated to annular regime are those conducted by Ong and Thome [22] and Revellin and Thome [18]. Revellin and Thome [18] predicted that as the channel size increases the transition occurs earlier, i.e., at lower vapor qualities and mass fluxes.

A unique test platform developed in our prior works [26,27] is utilized here to study the physics of transition process from the elongated bubbles to the annular flow regime. In the following sections, first, the test platform is presented. The experimental data consisting of thermal signature of different flow regimes along with synchronized images of the flow field are presented. The results on unique thermal characteristics of different flow regimes are discussed.

EXPERIMENTAL APPARATS AND MEASUREMENT

A schematic of the experimental device and a detailed view of the microfluidic chip are shown in Fig. 1. The device consists of a single rectangular microchannel with a cross-section height and width of 75 μm and 300 μm, respectively, made within a microfluidic chip fabricated on a silicon wafer through a multi-step microfabrication process. The microchannel is sealed by a Polydimethylsiloxane (PDMS) transparent cap. The microfluidic chip is fabricated on a silicon wafer through a multistep microfabrication process. Using a piezoelectric micropump (Model MP6, manufactured by Bartels Mikrotechnik GmbH), FC-72 as the working fluid is delivered to the test channel.

As shown in Fig. 1, the bottom surface of the test channel is a composite wall made of a thick high thermal conductivity

material (a 500 μm thick silicon substrate) coated with a low-conductivity (low-k) film (a 9.8 μm thick SU8 layer). A total of 53 platinum resistance temperature detectors (RTDs) are sputter deposited at the fluid-SU8 and SU8-silicon interfaces to measure the temperature distribution during the boiling process. The thickness of the sputtered platinum layer is 120 nm. Several thin film heaters are also embedded at the SU8-silicon interface. The sensors and the heaters have a 50-nm-thick titanium adhesion layer and gold bond pads. The RTD sensors are 50 μm wide and are placed 15 μm apart in the flow direction. The microfluidic chip is then wire bonded to a custom-made double-sided printed circuit board (PCB) before connecting to a high-speed data acquisition (DAQ) system (cf. Fig. 2)

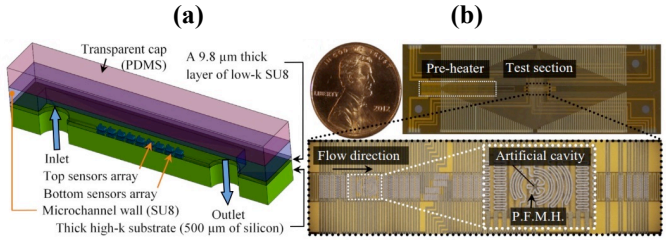

Fig. 1. (a) A schematic of the experimental device, (b) a detailed view of the microfluidic chip (test section, pre-heater, artificial cavity and pulsed function microheater)

The DAQ system which consists of a current excitation module (NI SCXI-1581), a channel amplifier module (i.e., signal conditioning module) (NI SCXI-1120C), a high-speed DAQ module (NI PXI-6289), and a programmable DC power supply module (NI PXI-4110) is commanded by an embedded controller (NI PXI-8115). The temperature data and the synchronized bubble images captured by a high-speed camera (FASTCAM SA4-Photron) are recorded at a rate of 20 kHz. In addition, the pulsed function microheater is connected to the programmable DC power supply module. Data collections as well as controlling the applied dc voltage to the pulsed function microheater are performed using a LABVIEW program. The thin film heaters are also powered by the NI PXI-4110 dc power supply.

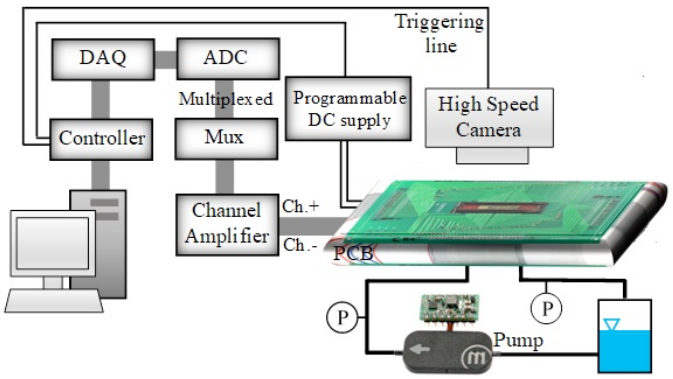

Fig. 2. Experimental setup used in this study

The RTD sensors are calibrated prior to the flow boiling experiments to obtain the voltage-temperature relationship of each sensor. The calibration tests are conducted in a uniform temperature oven over a temperature range of 40 ºC to 90 ºC. A constant current excitation of 100 μA is supplied to each sensor. The temperature sensors have a negligible self-heating. The recorded voltage-temperature curves show a linear relation and the sensitivity of the RTD sensors, the slope of the V-T curves, is 0.13 mV/ºC. The data acquisition system has a maximum uncertainty of ±28 μV, at a gain of 100 with a minimum detectable voltage change of 1 μV. Considering the sensitivity of the sensors and the voltage uncertainty, the maximum error in temperature measurements is determined to be ±0.25 ºC. In addition, the maximum uncertainty in the measurement of the SU8 film thickness and the local heat flux data are ±0.01 μm and ±1 W/cm^2, respectively [10].

RESULTS & DISCUSSION

The experimental data are recorded over a mass flux range of 109-250 kg/m^{2}s. Fig. 3 shows representative images of different flow regimes (left) and their respective schematics (right).

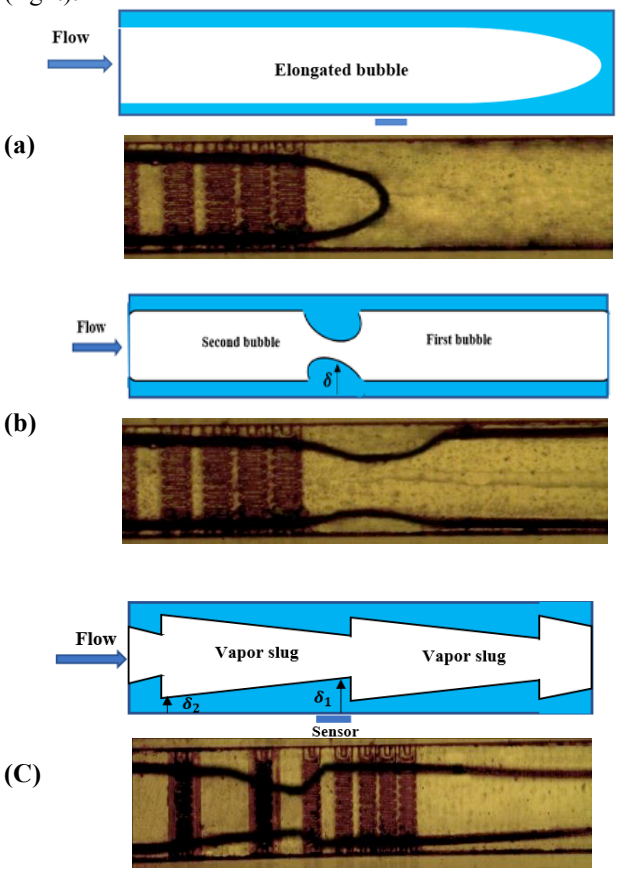

Fig. 3. Images and schematics of (a) elongated bubbles, (b) coalescing bubbles, and (c) semi-annular regimes.

The temperature signature associated with these regimes are provided in Fig. 4. In the elongated bubbles regime, two major modes of heat transfer can be readily recognized as the bubble moves over the sensor, namely: thin film evaporation, and transient heat conduction (cf. Fig 4a). A detailed discussion about these modes of heat transfer is available in our prior studies [26,27]. Fazeli et al. [27] provide a comprehensive analysis of the thin film formation and

evaporation process. The second temperature drop is due to the transient conduction process associated with the arrival of a liquid slug on the dried surface.

Increase in the bubbles velocity and their coalescence result in a fundamentally different surface temperature variations compared to that of a single bubble (cf. Fig. 4b). Also in this case, the transient conduction mode of heat transfer does not occur because the surface experiences no dryout.

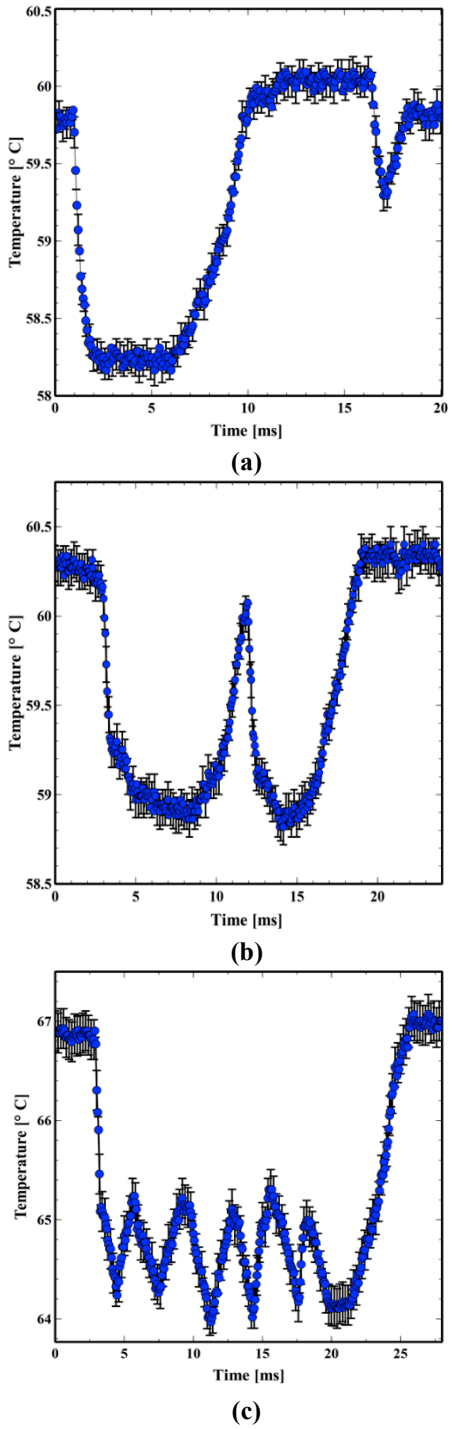

Fig. 4. Surface temperature for different flow regimes: (a) elongated bubbles, (b) coalescing bubbles, (c) semi-annular

The corrugation pattern of the temperature for the semi-annular regime suggests a periodic variation in the film thickness over the sensor (cf. Fig. 4c). The first drop in the temperature is due to the first liquid layer forming over the sensor when the surface has been dried for some milliseconds. The minimum temperature after the first drop corresponds to the thinnest film and then a fresh thick liquid layer arrives over the sensor resulting in a sudden temperature jump. This phenomenon occurs intermittently until a chain of fast moving vapor slugs passes and the sensor experiences complete dryout again.

Temperature signatures of two neighboring sensors spaced 60 μm apart are compared in Fig. 5. Comparison of the results indicates that the temperature profiles almost coincide for the elongated bubble regime while there is a time difference between the temperature profiles in the semi-annular regime (cf. Fig. 5b). Since the temperature drop is due to rewetting of the sensors, the time difference between the temperature drops of the neighboring sensors suggests that the thin film moves from one sensor to another. This renders the most important criterion for transition from the elongated bubbles to annular

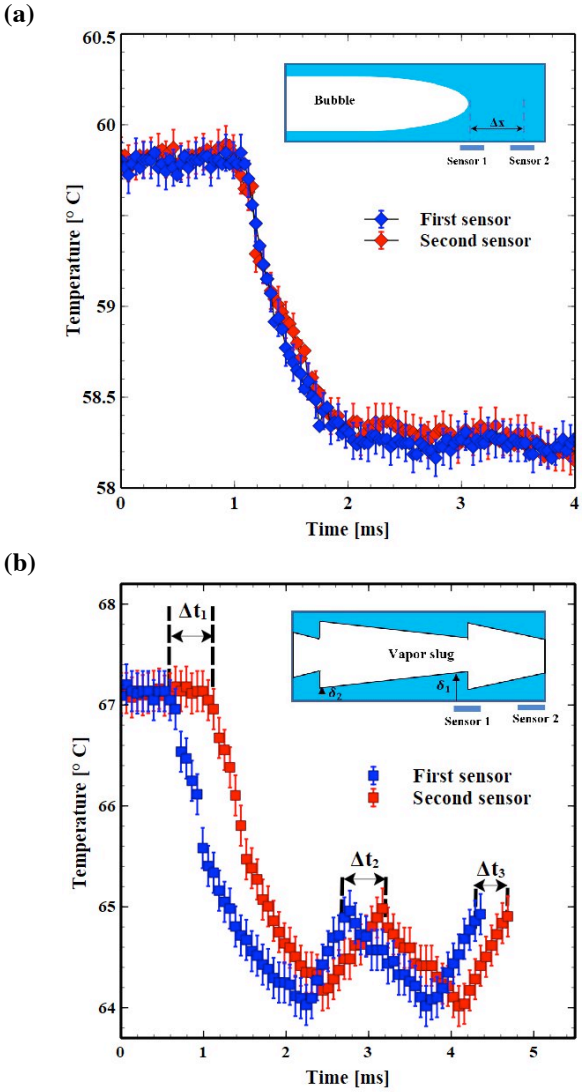

Fig. 5. Delay in temperature drop for two consecutive sensors: (a) Elongated bubbles (b) Semi-annular

flow regime that is a drastic variation in the liquid film velocity. Therefore, the distinction between the temperature profiles can be used to characterize the flow regime transition. As shown in our prior studies [26,27], the liquid film is extremely thin and forms and evaporates very rapidly making the characterization of its thermohydraluics difficult, however, we can characterize the thermohydraulic of the film with no limitation. On the other hand, the velocity measurement is possible just if there is a partial dry-out after which the liquid comes and rewets the sensors and then the film velocity can be characterized using the abrupt drop in the surface temperature. This is possible as long as we are in an intermittent regime that is semi-annular here.

As it is schematically indicated in Fig. 3c, before the chain of vapor slugs with liquid film around them arrive at the sensor, the surface of the sensor is almost dry, showing the highest temperature. Once the liquid arrives over the sensor, the temperature drops abruptly. Then, if the temperature drop for a sensor occurs at time t_1 and the next sensor records the temperature drop at t_2, the time that is required for the liquid film to move between the two sensors is t_2-t_1. Therefore, the velocity of the liquid film is $V=\Delta x/\Delta t$, with Δx being the distance between the two neighboring sensors.

Using the above-mentioned technique, the velocity of liquid film is calculated and compared for two different values of surface temperature as it is illustrated in Fig. 6. Increasing the mass flux affects the velocity in two ways. One portion of the added liquid mass evaporates and then increases the vapor velocity. The vapor with a higher velocity produces a larger drag force on the liquid film along the channel. In addition, the portion of the added liquid flow that is not evaporated increases the fraction of liquid in the cross section thickening the liquid film around the bubble. This thicker liquid film is subjected to weaker wall shear forces. As the surface temperature jumps, the liquid film moves faster because the rate of evaporations increases and the shear forces of the vapor slugs on the liquid film are augmented.

In prior studies, transition to the annular flow has been observed at very high mass and heat fluxes, however, it was unknown that why the flow exhibits such a different pattern that has a fundamentally distinct behavior from the slug and elongated bubble regimes. The main reason that at higher mass and heat fluxes the transition to the annular flow regime takes place is that the velocity of the liquid is high enough to incessantly flow along the channel. At such conditions the channel wall is readily wetted.

CONCLUSIONS

A novel experimental platform was developed to capture microscale physics of flow boiling transitional regimes. This development has provided an opportunity to measure the velocity of the extremely thin and fast moving liquid films in microchannels, for the first time. The precision of our tools allow us to measure the liquid film thickness underneath the vapor with no limitation. The velocity measurement is possible just if there is a partial dry-out after which the liquid comes and rewets the sensors and then the film velocity can be characterized using the abrupt drop in the surface temperature. This is possible as long as we stay in an intermittent regime,

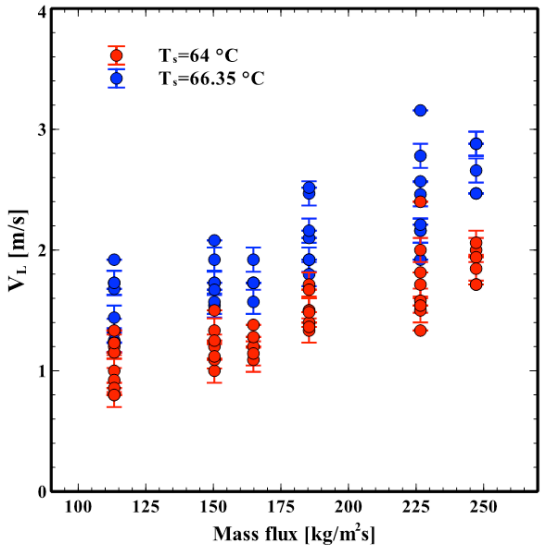

Fig. 6. Thin film velocity versus mass flux and surface temperature

that is semi-annular here. The experimental results showed that each flow regime has a unique thermal signature associated with the onset of the liquid film flow. This can be considered as the most fundamental mechanistic-based transition characteristic. Based on the velocity measurements, the results signify that the most important criterion of the flow regime transition from the elongated bubbles to the annular flow is the drastic variation in the liquid film movement.

ACKNOWLEDGMENTS

This study was supported by a grant from the National Science Foundation (NSF) under contract CBET-1403657. Fabrication of the devices was conducted in the Nanoscale Research Facility (NRF) at the University of Florida.

References

[1] J.R. Thome, Boiling in microchannels: a review of experiment and theory, Int. J. Heat Fluid Flow 25 (2004) 128–139.

[2] D. Li, G.S. Wu, W. Wang, Y.D. Wang, D. Liu, D.C. Zhang, et al., Enhancing flow boiling heat transfer in microchannels for thermal management with monolithically-integrated silicon nanowires, Nano Lett. 12 (2012) 3385–3390.

[3] V. Khanikar, I. Mudawar, T. Fisher, Effects of carbon nanotube coating on flow boiling in a micro-channel, Int. J. Heat Mass Transfer 52 (2009) 3805–3817.

[4] A. Kos_ar, C.-J. Kuo, Y. Peles, Boiling heat transfer in rectangular microchannels with reentrant cavities, Int. J. Heat Mass Transfer 48 (2005) 4867–4886.

[5] S.S. Mehendafe, A.M. Jacob, S.S. Mehendale, R.K. Shah, A.M. Jacobi, Fluid flow and heat transfer at micro- and meso-scales with application to heat exchanger design, Appl. Mech. Rev. 53 (2000) 175–193.

[6] S.G. Kandlikar, History, advances, and challenges in liquid flow and flow boiling heat transfer in microchannels: a critical review, J. Heat Transfer 134 (2012) 034001.
[7] S.G. Kandlikar, Fundamental issues related to flow boiling in minichannels and microchannels, Exp. Therm. Fluid Sci. 26 (2002) 389–407.
[8] A.M. Jacobi, J.R. Thome, Heat transfer model for evaporation of elongated bubble flows in microchannels, J. Heat Transfer 124 (2002) 1131–1136.
[9] T. Harirchian, S.V. Garimella, Flow regime-based modeling of heat transfer and pressure drop in microchannel flow boiling, Int. J. Heat Mass Transfer 55 (2012) 1246–1260.
[10] S. Bigham, S. Moghaddam, Microscale study of mechanisms of heat transfer during flow boiling in a microchannel, International Journal of Heat and Mass Transfer 88 (2015) 111–121.
[11] S. Bigham, S. Moghaddam, Role of bubble growth dynamics on microscale heat transfer events in microchannel flow boiling process, Applied Physics Letters 107, (2015) 244103.
[12] P. Zhang, H.W. Jia, Evolution of flow patterns and the associated heat and mass transfer
characteristics during flow boiling in mini-/micro-channels, Chemical Engineering Journal 306 (2016) 978–991.
[13] W. Wibel, U. Schygulla, J. J. Brandner, Micro device for liquid cooling by evaporation of R134a, Chemical Engineering Journal 167 (2011) 705–712.
[14] A. Sitar, I. Sedmak, I. Golobic, Boiling of water and FC-72 in microchannels enhanced with novel features, International Journal of Heat and Mass Transfer 55 (2012) 6446–6457.
[15] W. Qu, I. Mudawar, Flow boiling heat transfer in two-phase micro-channel heat sinks—I. Experimental investigation and assessment of correlation methods, International Journal of Heat and Mass Transfer 46 (2003) 2755–2771.
[16] T. Harirchian, S. V. Garimella, Effects of channel dimension, heat flux, and mass flux on flow boiling regimes in microchannels, International Journal of Multiphase Flow 35 (2009) 349–362.
[17] N. Kattan, J.P. Thome, D. Favrat, Flow Boiling in Horizontal Tubes: Part 1—Development of a Diabatic Two-Phase Flow Pattern Map. J. Heat Transfer 120, 140 (1998).
[18] R. Revellin, J.R. Thome, Experimental investigation of R-134a and R-245fa two-phase flow in microchannels for different flow conditions. Int. J. Heat Fluid Flow 28, 63–71 (2007).
[19] S. Garimella, J.D. Killion, J. W. Coleman, An Experimentally Validated Model for Two-Phase Pressure Drop in the Intermittent Flow Regime for Circular Microchannels. J. Fluids Eng. 124, 205 (2002).
[20] C.L. Ong, J.R. Thome, Flow boiling heat transfer of R134a, R236fa and R245fa in a horizontal 1.030mm circular channel. Exp. Therm. Fluid Sci. 33, 651–663 (2009).
[21] C.B. Tibiriçá, G. Ribatski, Flow patterns and bubble departure fundamental characteristics during flow boiling in microscale channels. Exp. Therm. Fluid Sci. 59, 152–165 (2014).
[22] C.L. Ong, J.R. Thome, Macro-to-microchannel transition in two-phase flow: Part 1 - Two-phase flow patterns and film thickness measurements, Exp. Therm. Fluid Sci. 35, 37–47 (2011).
[23] C.B. Tibiriçá, G. Ribatski, Flow Boiling in Micro-Scale Channels – Synthesized Literature Review International Journal of Refrigeration 36, no. 2 (2013): 301–324.
[24] L. Cheng, G. Ribatski, J.R. Thome, Two-Phase Flow Patterns and Flow-Pattern Maps: Fundamentals and Applications, Applied Mechanics Reviews 61, no. 5 (2008): 50802–50828.
[25] Triplett, K. A., Ghiaasiaan, S. M., Abdel-Khalik, S. I., and Sadowski, D. L. "Gas–liquid Two-Phase Flow in Microchannels Part I: Two-Phase Flow Patterns" International Journal of Multiphase Flow 25, no. 3 (1999): 377–394.
[26] S. Bigham and S. Moghaddam, "Physics of the Microchannel Flow Boiling Process and Comparison With the Existing Theories," *J. Heat Transfer*, vol. 139, no. 11, p. 111503, Jun. 2017.
[27] A. Fazeli, M. Habibi Matin, S. Moghaddam, Physics of Microlayer Formation in Microchannels: New Physical Insights and Governing Correlations, 2018 IEEE ITherm, San Diego, CA, USA.